Structural Monitoring for the Cyclic Behaviour of Concrete Tunnel Lining Sections Using FBG Sensors

Oreste S. Bursi[1], Nicola Tondini*[1], Manuel Fassin[1], Alessio Bonelli[1]

[1]*University of Trento, ITALY, Department of Civil, Environmental and Mechanical Engineering*

Published at:
Bursi O.S., Tondini N., Bonelli A. and Fassin M. (2016) Structural monitoring for the cyclic behaviour of concrete tunnel lining sections using FBG sensors, Structural Control and Health Monitoring, 23(4):749-763, doi: 10.1002/stc.1807.*

Abstract: *To demonstrate the viability of using Fibre Bragg Grating (FBG) sensors capable of detecting the inelastic cyclic response of reinforced concrete sections that are part of tunnel linings, an experimental research programme carried out on different packaging configurations of FBG sensors is presented in this paper. The programme illustrated here was part of a wider research project funded by the European Commission whose objective was the development of a Decision Support System (DSS) for monitoring tunnel linings in seismic-prone regions. In particular, a typical metro tunnel located in the Rome area, Italy, was considered as a case study. In order to provide useful information for designing an effective sensor packaging to be applied to a final full-scale test representing a whole lining circular section of a tunnel, pure bending tests were designed and performed on five substructure specimens endowed with different sets of fibre packaging. The outcomes of the substructure tests showed that the optimal FBG packaging solutions were unbonded sensors either embedded in concrete or mounted externally. Moreover, the designed fibre sensor system reliably performed at large deformations. In fact, the external FBG fibres applied to the full-scale tunnel test approached maximum values of about 0.63 per cent, whilst the internal fibres reached about 1.2 per cent. The results obtained by FBG sensors were in good agreement with those of traditional transducers.*

Keywords: Structural health monitoring, FBG sensors, Tunnel linings, Seismic zones, Inelastic sections

1 INTRODUCTION

Due to the advancements in construction techniques and sensing technology [1], tunnels constitute an easier and efficient transportation solution in already congested cities and hilly regions. Nonetheless, the modern transport networks demand longer and wider tunnels being

driven through increasingly difficult ground conditions. Nowadays, many railway, road and metro-line tunnels are under construction in densely populated seismic-prone areas and require high level of safety. In fact, tunnels have shown increased sensitivity to seismic loadings with significant damage in recent large earthquakes including the 1999 Kocaeli, Turkey earthquake, the 1999 Chi-Chi, Taiwan earthquake and the 1995 Kobe, Japan earthquake [2]. In the case of railway and metro tunnels, even moderate deformations of the track may cause vehicle derailing. Moreover, it is quite difficult to assess both damage and residual capacity of a tunnel after a major earthquake followed by aftershocks.

A tunnel could be stressed in several modes owing to an earthquake; however, seismic shear waves that propagate approximately transversely to the lining axis entail the maximum damage owing to the ovalization of the original circular section ([3], [4], [5] and [6]). Herein, we considered circular sections, which are obtained by machine-boring and are mainly used for important infrastructures. The majority of theories used to determinate the soil distortion in the ground considers the free field deformation approach [7], where the presence of both lining and cavity is neglected.

During a significant earthquake event, the tunnel lining is subjected to large deformations. Since tunnel linings are built in reinforced concrete, their non-linear behaviour is certainly activated, with formation of localized plastic hinges. In these conditions, the adoption of a robust structural monitoring system made of distributed optical sensors could be very useful to measure average strains and temperatures [8]. In particular, FGB systems are experiencing a rapid development owing to their inherent distinctive advantages such as small size for local measurements, light weight, immunity to electromagnetic interference and corrosion, and embedding capabilities. Thus, they have been successfully applied in diversified engineering fields, including civil and geotechnical engineering [9], [10], oil and gas [11], damage detection [12], etc.

FBG sensors strongly meet the requirements for monitoring the structural health of an underground structure because: i) they are capable of providing high-resolution strain information at specified points of a structure, and ii) they can be arranged in cascade to form a distributed system of sensors along a common fibre optical cable which can be simultaneously interrogated through a single source/detection unit. Dedicated fibre cables and FBG arrays can independently monitor several different parts of the same structure by reusing the same optical spectrum. Additionally, FBG sensors exhibit high sensitivity, excellent reproducibility reliable stability and insensitivity to harsh environmental conditions, such as corrosion, humidity, electromagnetic fields, etc. In addition, quite accurate instruments can be designed by means of FBG sensors [13].

With regard to concrete structure monitoring by means of FBG fibres, they are widely employed for cracking, vibration control and applications with different measurands such as strains, deflections/displacements, accelerations, etc ([14], [15], [16], [17]). In greater detail, a common measurement range for reinforced concrete structures is $\pm 1000 \div \pm 5000$ microstrain ([18], [19]). As a result, given the favourable characteristics listed above, a FBG sensing system could capture the inelastic cyclic deformations of lining tunnel sections.

The MONICO project was funded by the European Union within the 7th research programme framework, to explore the feasibility of tunnel monitoring by means of optical fibre sensing technology. Its main objective was to ensure the safety of seismic-vulnerable

tunnel cross-sections where very high standards of safety are required, by developing a DSS that relies on information provided by fibre optic sensors; thus, real-time assessment of the structural reliability of the tunnel lining should be guaranteed [20]. In order to obtain a reliable and robust monitoring system, the pursuit of an optimal fibre packaging to be applied to critical tunnel sections was sought. For this purpose, we aimed at reaching a target strain range of ±10000 microstrain (1%), identified as adequate for capturing the nonlinear behaviour of ductile concrete sections in moderate seismic-prone areas. Hence, experimental tests on substructures equipped with different fibre packages were performed on a segment of tunnel lining taken as case study. The design of this optimal fibre packaging configuration represented the main focus of this study, which also included details and features of the whole experimental campaign carried out on substructures. Some results on the full-scale tunnel lining test are also presented in order to show the effectiveness of the FBG packaging optimization process performed in the substructure test programme. Nonetheless, more detailed information about this test and relevant damage estimation provided by FBG sensors can be found in a separate study [21].

2 THE TUNNEL LINING CASE STUDY

In the MONICO project, a benchmark tunnel lining with a circular hollow section was selected. The tunnel location was considered in the Rome area, Central Italy. The outside diameter was 4.8 m, the lining thickness 0.2 m and the tunnel axis was located at 20 m below ground level. The elastic modulus and the Poisson coefficient of the lining concrete were assumed to be 31.4 GPa and 0.2, respectively. With regard to soil properties, the elastic modulus and the Poisson coefficient were set to 84 MPa and 0.49, respectively, and the height of the water table above the lining to 5 m. The density of the soil was 1800 kg/m^3 and the overload 2 kN/m^2. The seismic action considered at the Life Safe Limit State (LSLS) was equivalent to a design reference peak ground acceleration (PGA) on type A ground (rock) of 0.16 g, as expected in Rome with a nominal life of 100 years; and an importance factor IV entailing a reference life of 200 years with a return period of 1898 years [23]. This induced a PGA in a type D ground (deposits of loose-to-medium cohesionless soil, S=1.752) of 0.28g; a peak ground particle velocity of 0.319 m/s [23]; and an effective shear wave propagation velocity of 125.1 m/s, determining a maximum soil shear strain of 0.26%. The latter value represented the input for the cross-section design. The relevant actions on tunnel were evaluated by means of the formulation proposed by Penzien and Wu [4] which takes into account also the effect of lining stiffness. As a result, lining stresses were computed for: i) self-weight of the soil, ii) overload, and iii) seismic deformation under the basic assumption of deep tunnel and homogeneous soil. As for seismic conditions, although the seismic wave propagation direction is mainly vertical, it can be inclined for shallow tunnels or near a fault. In particular, the worst case for structural safety of a lining occurs when seismic waves propagate at an angle of 45° because the peak values resulting from seismic and from static actions sum up. Moreover, in the Penzien's relationships [4], it was assumed that no soil deformation occurs as a consequence of the tunnel boring method and that a condition of full slip between soil and tunnel was achieved. As a result, the overall stress

state derives from the combination of the three basic loads described above. The typical distribution of internal forces is a crossed sinusoid, see Figure 1, where the maximum moment was reached at 0°, 90°, 180° and 270°. The maximum and minimum force values are gathered in Table 1. The bending moment distribution obtained using the Penzien's method [4] is characterized by a sinusoidal shape that exhibits a low gradient around the maximum and minimum moment, i.e. in the plastic hinge region whose length is estimated in Subsection 3.1.1. Hence, this region can be treated as at constant moment, as shown in the enlargement of Figure1b. In fact, the reader can observe that the maximum moment amplitude ($\Delta M/M_{max}$) varies along the circular tunnel lining less than 15% over one meter of length.

With both static and LSLS seismic load combinations, it was found that the tunnel cross-section was satisfactory with a 50 mm C25/30 concrete cover and 7+7 ϕ16 B450 C reinforcing bars, as shown in Figure 2a. In addition, Figure 2b illustrates the moment-curvature diagram of the section associated with the maximum and minimum thrust. As expected, compression increases the strength of the section but decreases ductility. Furthermore, the moment-curvature diagram allowed for estimation of the curvature demand under seismic loading and also to check whether FBG sensors were actually capable of measuring strains beyond yielding.

Table 1

Maximum and minimum characteristic values of internal actions based on Penzien and Wu theory [4]

Stress	Max	Min
Bending moment [kNm/m]	84.38	-84.38
Thrust force [kN/m]	-640.25	-780.89
Shear action [kN/m]	69.25	-69.25

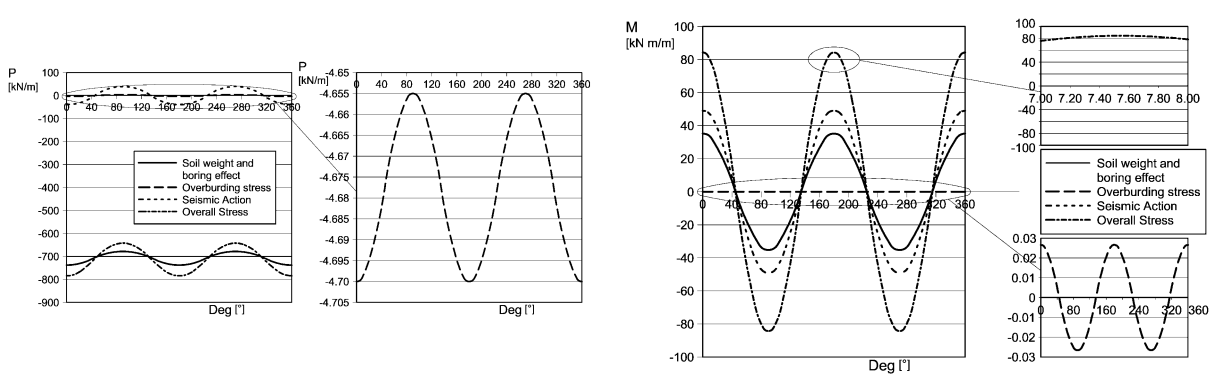

(a) (b)

Figure 1 Actions estimated by means of the Penzien and Wu [4] formulae: a) thrust values, and b) bending moment values.

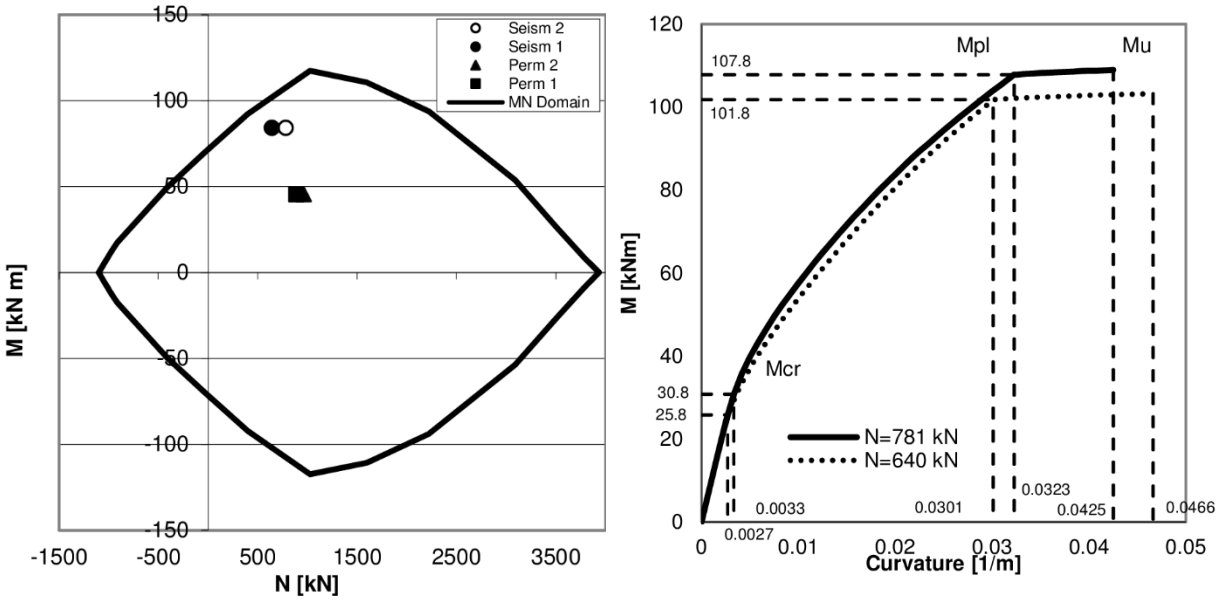

(a) (b)

Figure 2 Strength of the transverse section under normal stresses: a) M-N diagram relevant to Static (Perm) and Seismic LSLS (Seism) actions, and b) Moment – Curvature diagram relevant to the maximum and minimum thrust action estimated by the Penzien and Wu [4] relationships

3 CONCRETE SPECIMENS AND EXPERIMENTAL PROGRAMME

3.1 Test Specimens

3.1.1 Substructure specimens. In order to quantify damage of tunnel linings [24], [25], [26] and [27], it is deemed necessary to estimate the length of concrete sections where inelastic phenomena localize, i.e. the plastic hinge length. This estimate entails a large dispersion, [28] and [29], and directly involved the fibre length to be used in the full-scale experiment mentioned hereinafter. Thus, to overcome these problems and to characterize the moment capacity and the plastic rotation of concrete sections, a test series on substructures was planned. Moreover, these tests helped into the selection of an optimal packaging for FBG sensors. In a greater detail, these tests were performed to gain information on: i) their optimal configuration, ii) their location, and iii) the length of fibres to be installed in each section. As a result, the same geometry, materials and pre-stressing forces foreseen in the full-scale test characterized the substructure specimens.

As shown in Section 2, the maximum bending moment over one meter of tunnel lining was almost constant at maxima. Therefore, in order to reproduce the fairly uniform bending stress as exhibited in areas of maximum values on substructure specimens, a four-point bending scheme was adopted. Both the cross-section of the specimens and the loading scheme are shown in Figure 3a and Figure 3b, respectively. Each specimen had cross-section

1000 mm x 200 mm and a length of 3000 mm. Concrete was of class C25/30 and (7+7) Φ16 B450C steel bars composed the reinforcement cage.

The relevant plastic hinge length l_{pl} was calculated with two different relationships. The estimates of l_{pl} were 16.5 cm and 48 cm, according to Nilson and Winter [28] and the Italian Seismic Code OPCM 3274 [29], respectively.

With regard to the testing set-up, the bending moment between loading points was imposed by increasing the vertical displacement through a hydraulic actuator, whilst the pre-stressing force, equal to 600 kN, was applied by means of a pair of pre-stressed dywidag rods. Since the plastic hinge length was estimated between 16.5 cm and 48 cm, the span between the two loading points for uniform bending moment was set to 40 cm. As a result, test data provided both flexural ductility and strength characteristics without any shear effect.

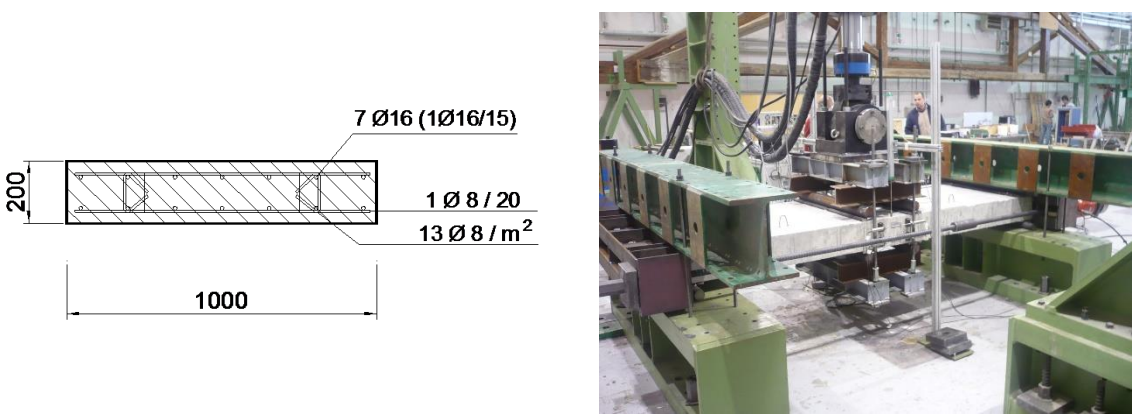

(a) (b)

Figure 3 Test set-up on substructure: (a) cross-section specimen; (b) four-point loading set-up.

3.1.2 Full-scale specimen. The full-scale specimen representing a whole tunnel lining section was extracted from the metro tunnel described in Section 2. In addition, in order to consider the worst case for tunnel lining structural safety, a seismic wave propagation direction at an angle of 45° was considered. This choice was applied through the test set-up shown in Figure 4, where two electro-hydraulic actuators were located orthogonally to one another.

The axial force was applied by means of steel ties supported by a system of cylindrical bearings. This arrangement proved to be the most efficient solution with respect to friction losses. The same load in substructure tests, i.e. 600 kN, was applied to the full-scale specimen using three 24 mm high-tensile steel cables, which were pre-stressed with two hollow jacks of 1000 kN capacity each. Then, the tensile force was transferred to the ring by vertical steel rollers. The ovalization of the section caused by the two hydraulic actuators offered a good representation of the stress states found in the literature [4], [2] and [6].

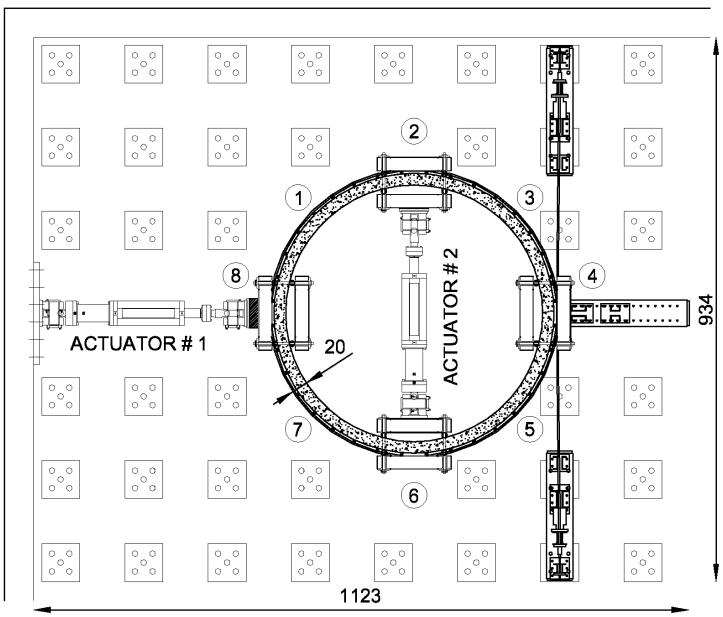

Figure 4 Plan of the tunnel lining TLC1 specimen and loading set-up. Dimensions in cm

3.2 Test programme and loading protocols

The experimental programme of the specimens described above was divided into two parts:

a) tests on substructures of the tunnel lining representative of concrete sections;
b) tests on a full-scale specimen representative of the whole tunnel lining.

Monotonic and cyclic tests relevant to substructures are listed in Table 2. In order to acquire the whole force-displacement response as well as the maximum ductility, a test under monotonic loading was performed in displacement control. Relevant results served to calibrate the subsequent cyclic tests.

Table 2 Test programme and Fibres combinations used in different tests

Test		*Testing Procedure*	*Specimen/Test acronym*	*Notes about fibres*
Substructure Tests	1	Monotonic	SSM1	No fibre
	2	Cyclic ECCS	SSC1	No fibre
	3	Cyclic ECCS	SSC2	Internal bonded and unbonded FBG fibres
	4	Cyclic ECCS	SSC3	External unbonded FBG fibres
	5	Cyclic ECCS	SSC4	Internal and external unbonded FBG fibres
	6	Cyclic ECCS	SSC5	External unbonded Brillouin fibres
Test on Tunnel Lining		Cyclic ECCS	TLC1	FBGs with various configurations

Cyclic tests were conducted by means of the ECCS procedure [30]. The relevant loading protocol is based on a conventional displacement δ_y, which represents the elastic-plastic transition of the cross-section behaviour. The ECCS cyclic loading protocol consists of a series of cycles in displacement control, which are increased proportionally to the δ_y value, as shown in Figure 5. In detail, the monotonic test on substructures provided a deflection of 19 mm at first yielding of reinforced bars; the specimen failed at a displacement of about 60 mm associated with high loss of stiffness and strength. In the cyclic test, it was decided to set a maximum displacement at $4\delta_y$ = 76 mm.
Given the size, only one full-scale specimen was available for testing the whole FBG system. Thus, only an ECCS-based cyclic test was performed. The estimate of $\delta_{y.ring}$ was based on the result of the substructure monotonic test SSM1. It resulted to be equal to ±30 mm for each of the four loaded sections. Other test details can be found in [21].

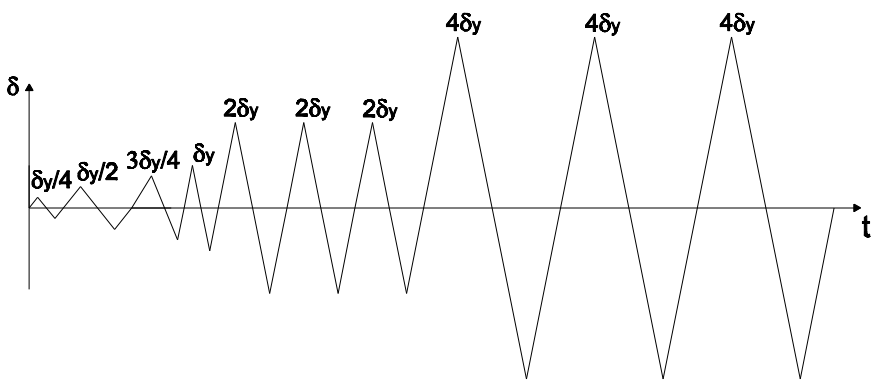

Figure 5 Loading protocol according to the ECCS procedure [30].

4 FIBRE PACKAGING

Based on concrete cross-section calculations of tunnel linings located in seismic areas, we estimated maximum tensile deformation demands in the cross section of about 1%. Thus, we focussed on the capability of FBG sensor of predicting the mechanical behaviour of instrumented sections in the nonlinear range up to a strain of at least 1%. In terms of wavelength shift, a maximum strain of 10000 με was translated to about 12 nm, assuming a typical silica FBG strain sensitivity of 1.2 pm/με. Since the strain sign - especially owing to seismic effects - can switch from positive to negative, the spacing between the Bragg wavelengths was doubled; thus, 24 nm of bandwidth were allocated per sensor. As the interrogation unit was endowed with spectral limits between 1515 nm and 1590 nm, respectively, i.e. a nominal operational wavelength range of 75 nm, to preserve the capability of sensing 1% deformation in both compression and tension, a maximum of 3 sensors per line was applied. The corresponding wavelength allocation is shown in Figure 6. Conversely,

the wavelength spacing of the temperature sensors was much smaller, about ±1 nm and ±2 nm, which was enough for measuring temperature changes over ±100°C.

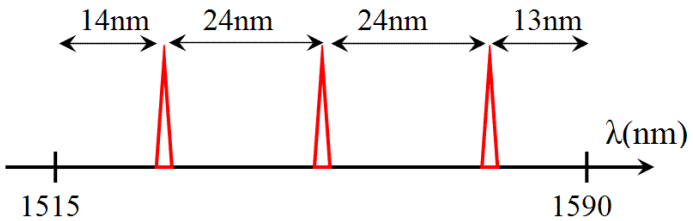

Figure 6 Spectral distribution of three strain FBG sensors in the 75 nm wavelength window. The sensor wavelengths were λ_1=1529 nm, λ_2=1553 nm and λ_3=1577 nm

4.1 Substructure specimens

Various FBG configurations were employed. In a greater detail, FBG sensors were attached to steel reinforcements of concrete: steel rebars or square steel rebar with a groove, either i) bonded to or ii) unbonded to concrete. Moreover, FBG sensors were externally mounted on metal holders welded to reinforcement bars through access holes left during casting.

The unbonded sensor solution was conceived because in a reinforced concrete element major cracks form at a spacing which is generally in the order of several centimetres. Rebars undergo plastic deformation only at cracks, whereas between two cracks they remain in the linear range. Thus, if the base length of the gauge measurement is very short, as it is for FBG fibres, the probability that a sensor spans a crack is very small, and consequently, it would measure the elastic strain of the steel rebar also for a cracked concrete case. In the unbonded solution, the strain measurement was obtained as an average over a long measurement base; thus, it was not influenced by local material discontinuities and inclusions. As a result, the latter measurement provided information related to *global* rather than *local* structural behaviour.

For the reinforced concrete section under study, the average crack spacing $s_{r,avg}$ was about 11 cm whereas the maximum spacing $s_{r,max}$ = 18 cm [31]. Thus, unbonded embedded fibre sensors were *decoupled* from concrete for a distance larger than $s_{r,max}$. The external FBG sensors were mounted by welding two steel plates to the rebar cage and again at a distance larger than $s_{r,max}$. The installation of external FBG fibres is convenient because it can be easily done after completion of the tunnel and replacement would be straightforward in the case of a fault. For the unbonded sensor solution, fibre pre-straining was needed with values between 0.76 - 0.88%. As a drawback, this type of installation needs to be attainable after the lining construction; therefore, proper section details must be conceived.

In sum, three types of solutions were tested: i) FBG installed on a special stirrup composed of two 10 x 10 mm steel bars inside a 3 mm groove, as shown in Figure 7a; in which the unbonded solution was achieved by fixing the fibres in the groove with a shore D 96 epoxy resin that was then filled with silicon; ii) FBGs externally installed, as depicted in Figure 7b;

iii) FBGs directly installed on the steel rebars of the specimen, as depicted in Figure 7c, or, in the case of the full-scale test in small rebars not influencing the section behaviour. In this third case, the unbonded solution was achieved by protecting the unbonded length with flexible material - foam with water protection or silicon. In addition to fibres and to check the reliability and accuracy of FBG sensors, all tests were monitored also by means of traditional sensors such as various type of Displacement Transducers, i.e. potentiometer DT, LVDT and strain gauges DT, inclinometers and strain gauges for concrete, as shown in Figure 8. The sensor packaging was accommodated in the zone where a plastic hinge formation was expected and the complete list of fibre packaging employed for each test is provided in Table 2.

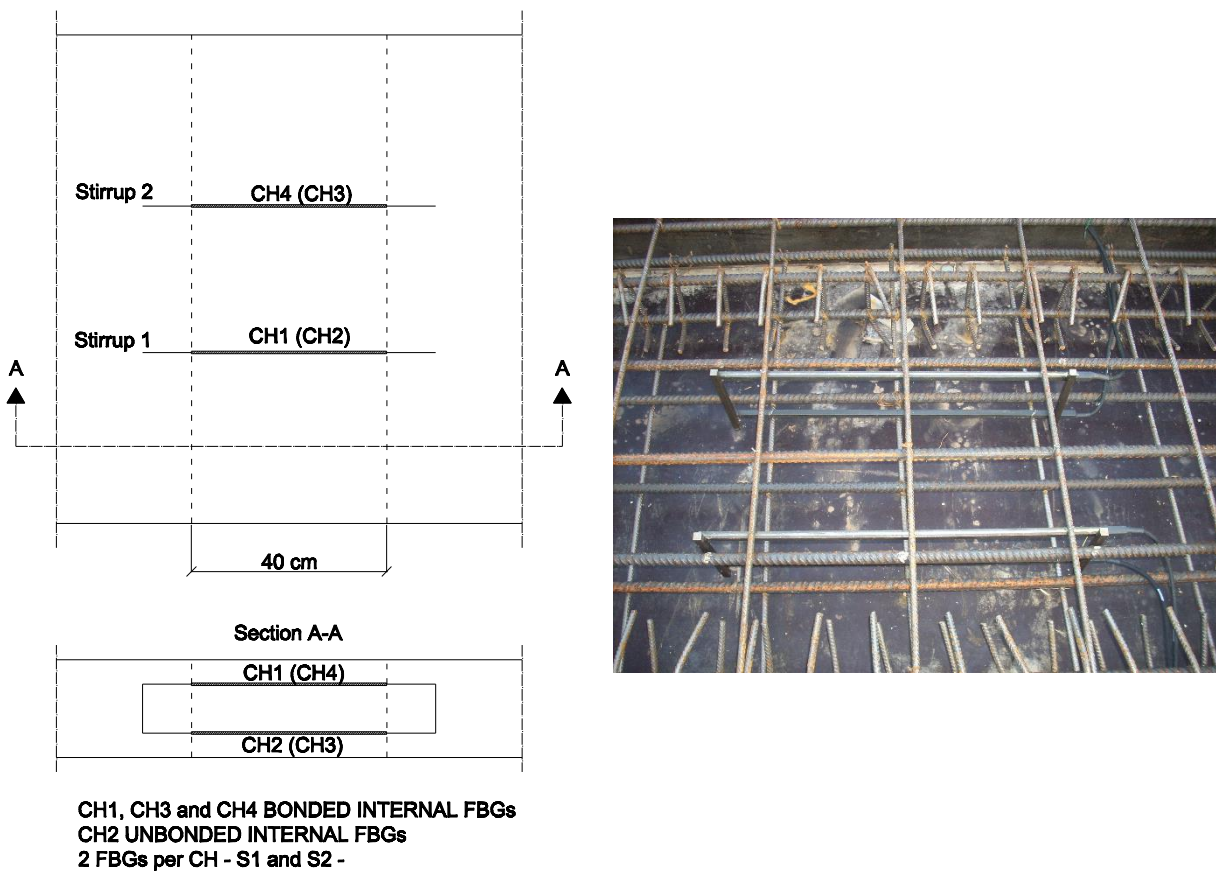

(a)

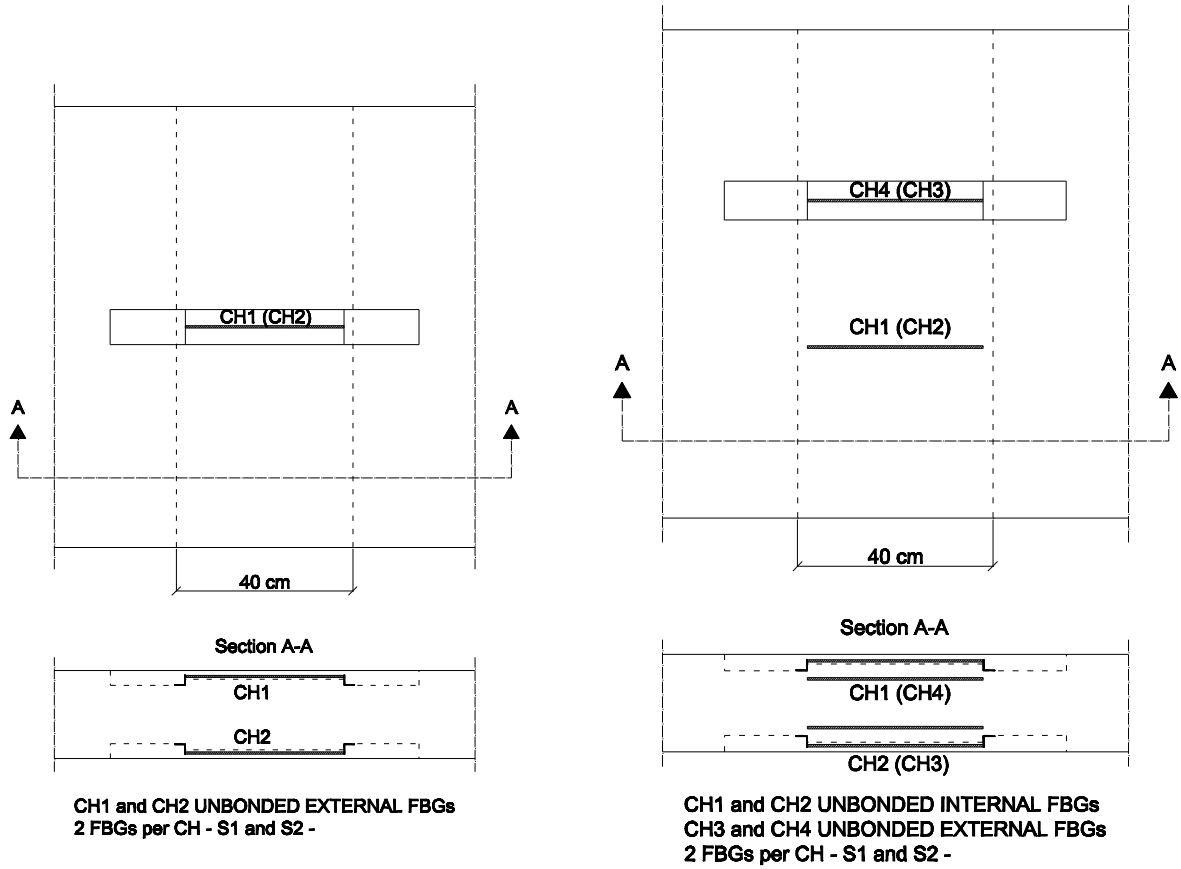

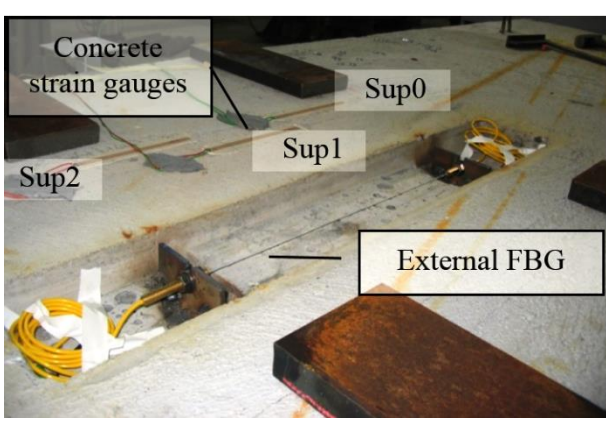

(b) (c)

Figure 7 FBG location in the uniform bending zone of the specimens: a) SSC2 – plan view, section view and picture before casting – ; b) SSC3 – plan view, section view and picture after casting –; c) SSC4 – plan view, section view and picture before casting –

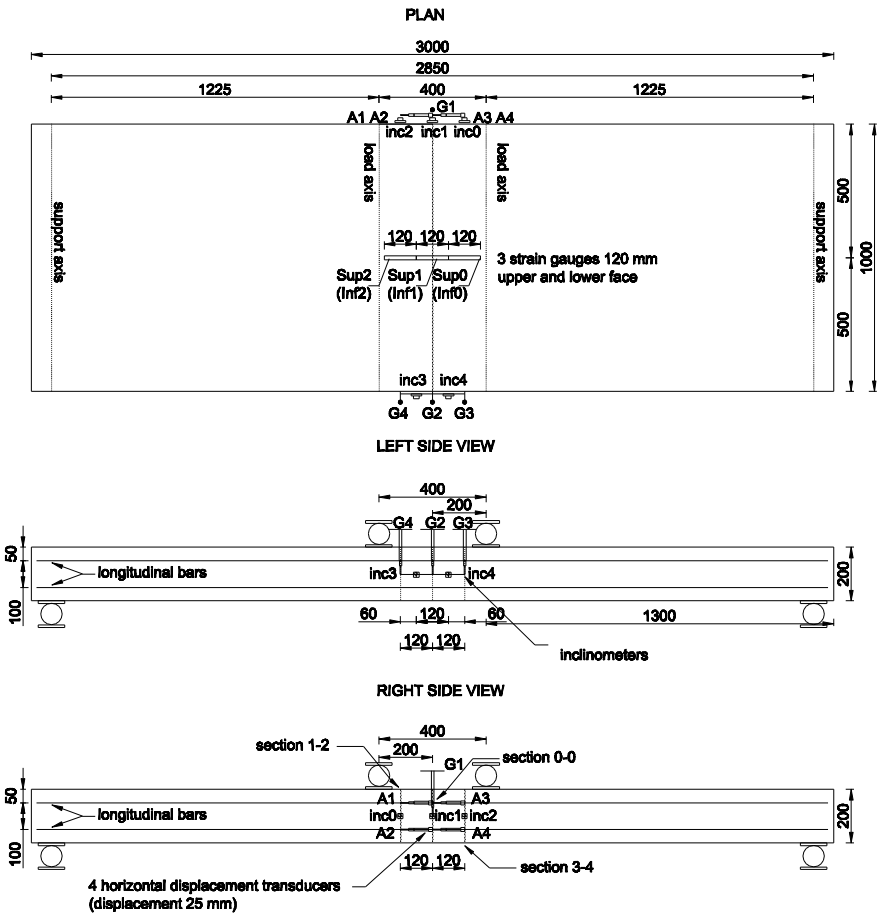

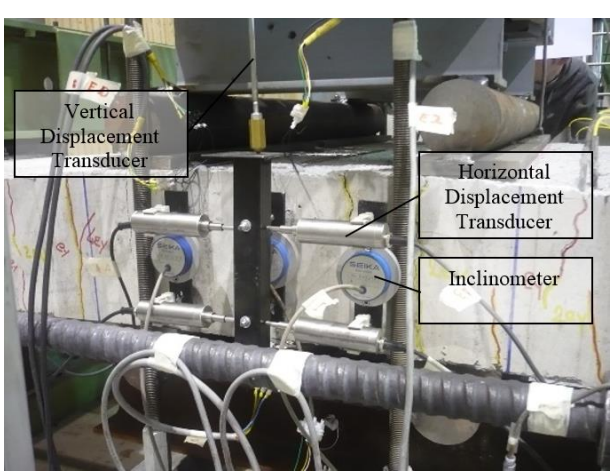

Figure 8 Location of horizontal displacement strain transducers, inclinometers and vertical displacement transducers in the SSC2 specimen. Dimensions in mm.

4.2 Full-scale specimen

The substructure tests provided the optimal fibre packaging that was then employed for the full-scale specimen. Nevertheless, to get a complete picture of all package capabilities, the tunnel ring was also instrumented with bonded fibres as illustrated in Figure 9. Taking also into account the temperature sensors that are needed to compensate for additional temperature-induced wavelength shifts of all fibres, the system for each monitored section consisted of 24 strain sensors and 16 temperature sensors. Moreover, standard devices were also added.

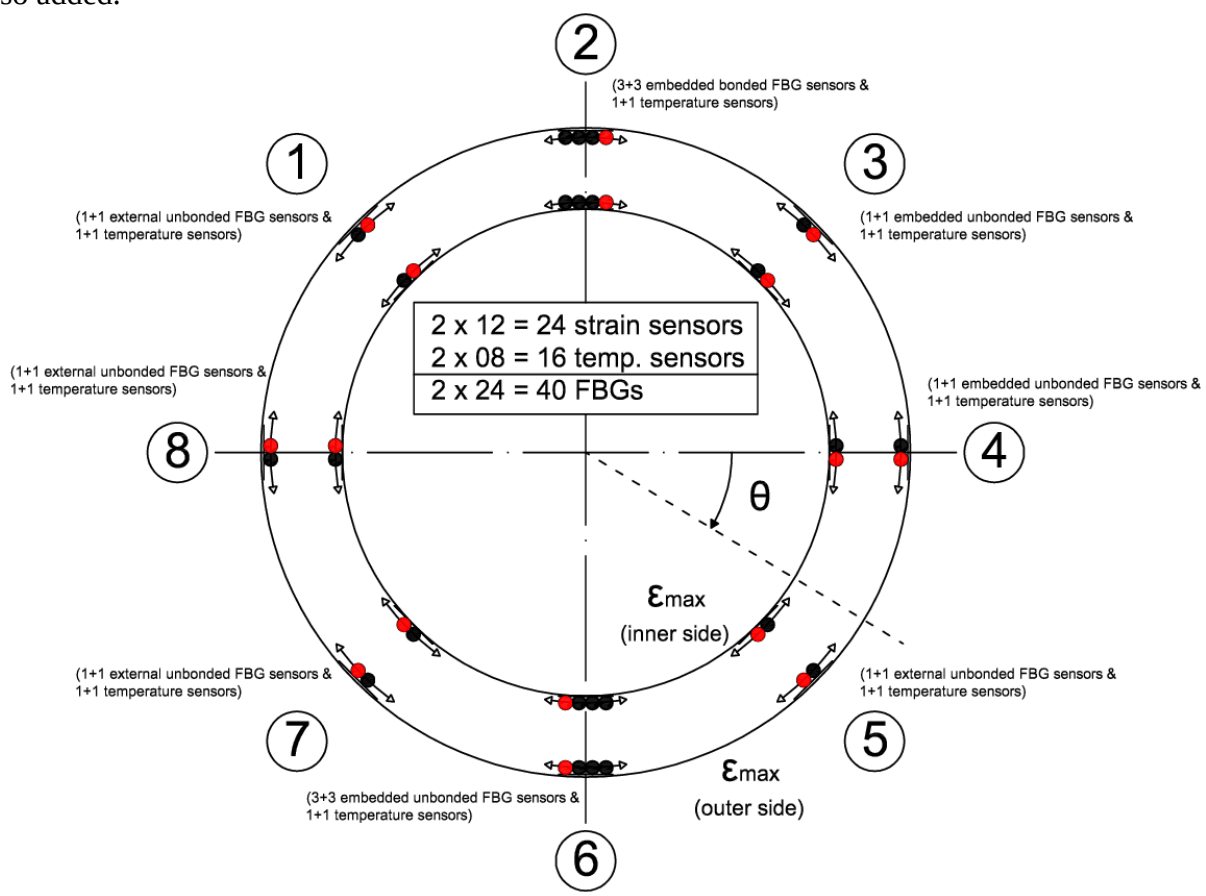

Figure 9 Direction and distribution of strain FBG sensors (black) and temperature FBG sensors (red) installed in the tunnel lining case study.

5 FBG RESULTS AND COMPARISON WITH STANDARD DEVICES

Test results on substructure specimens are summarized herein, and the most significant results relevant to fibre behaviour are highlighted. In particular, the SSC2, SSC3 and SSC4 tests listed in Table 2 were selected. SSC2 test showed the behaviour of internal bonded and unbonded fibres installed by means of steel stirrup with a square section with a groove, as depicted in Figure 7a, whereas both the SSC3 and SSC4 provided insight on the performance of the external packaging solution.

Both the moment-rotation curve and the moment-curvature relationship relevant to the SSC2 specimen are shown in Figure 10, where in the legend *1c* $\delta_y/4$ stands for "first cycle at displacement amplitude $\delta_y/4$" and so on. In detail, plots are obtained from the signal acquired from standard devices -rotation was evaluated from inclinometers whilst curvature from the horizontal displacement transducer assuming plane sections-. Some asymmetry owing to material imperfections was observed. Moreover, favourable hysteretic behaviour owing to large energy dissipation is evident. Thus, this cross section appeared suitable for seismic applications. The relevant responses of bonded and unbonded fibre sensors for the lower beam face are shown in Figure 11, where S1 and S2 represent signals acquired from the two FBGs installed in the same side of the section as shown in Figure 7a.

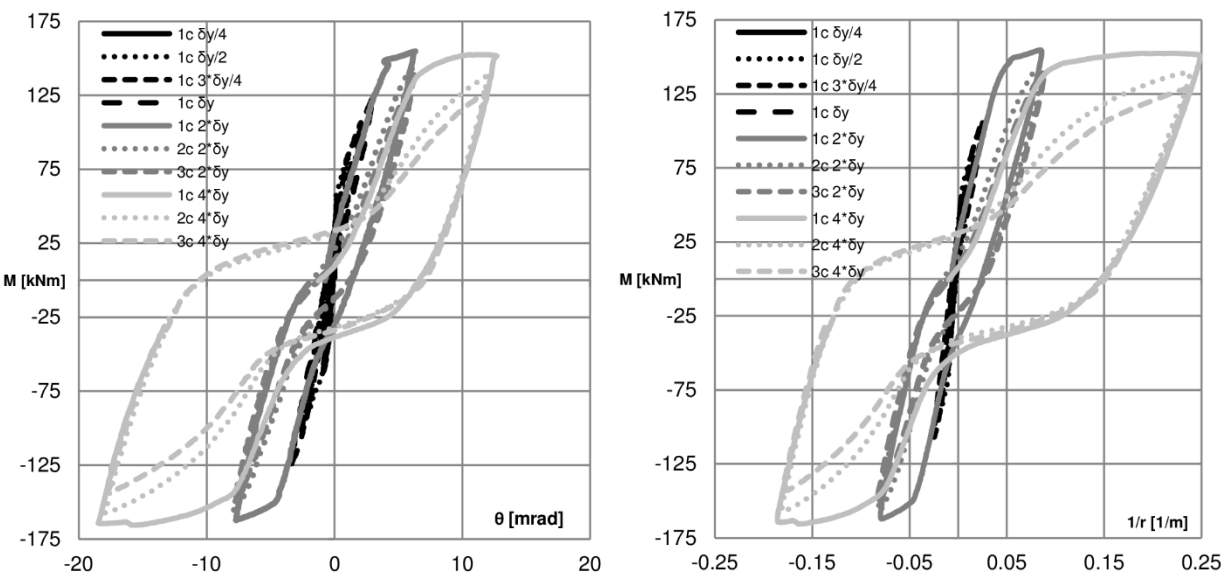

(a) (b)

Figure 10 SSC2 test: a) moment–rotation curve, and b) moment–curvature relationship obtained from strain gauge displacement transducers

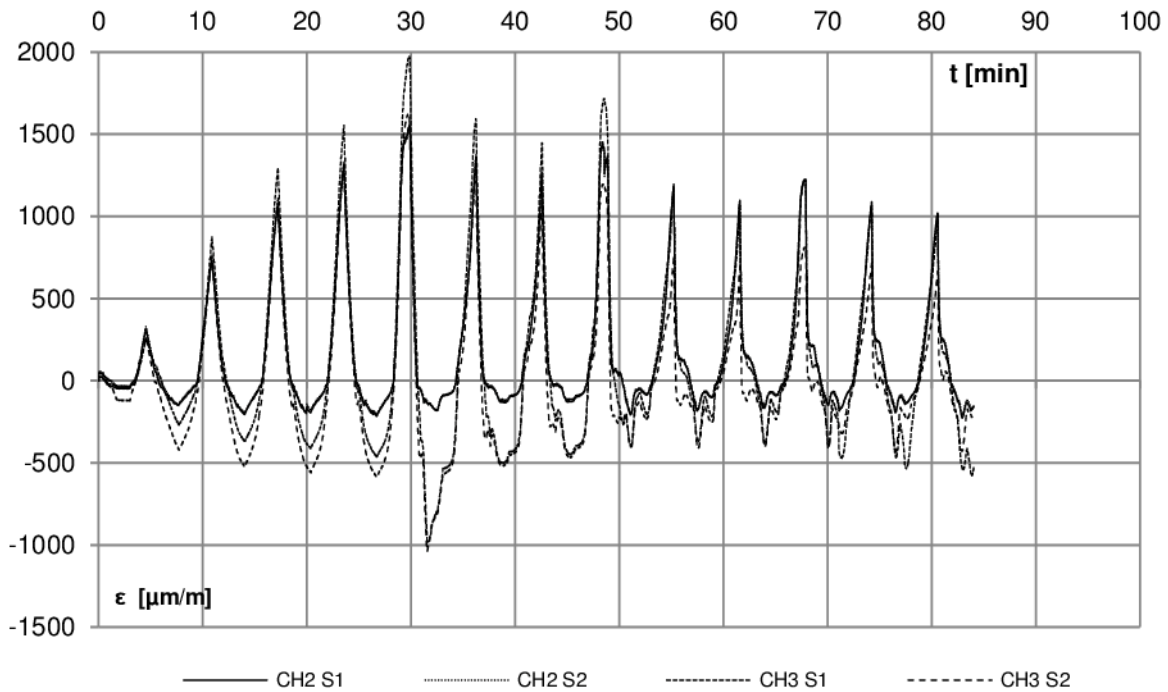

Figure 11 SSC2 test: strain values provided by unbonded (CH2) and bonded (CH3) fibre optic sensors located on the bottom side of the beam

From Figure 11, a careful reader can note that both unbonded and bonded internal packaging solutions for fibres were not capable of detecting 1% strain values. In particular, FBGs were not capable of reliably measuring strains beyond $2\delta_y$; in fact, the strain magnitude detected reduced after the first cycle at $2\delta_y$. This behaviour was probably caused by detachment of the stirrups from the concrete owing to cracking. Moreover, the deformation in compression (-) was always less than that detected in tension (+), as cracks opened under tension. Up to the first half $2\delta_y$ cycle, the strain state of the cross-section was estimated by relying on data provided by: i) displacement transducers (AEP), ii) strain gauges and iii) bonded FBGs, by assuming plane sections and a perfect bond between concrete and rebars. The relevant graphs are shown in Figure 12. It is evident: i) a plastic behaviour from AEP readings; ii) a plastic behaviour from strain gauge readings; and iii) an elastic behaviour from fibre readings. Strain values read by AEPs and by strain gauges were obtained as an average on a measurement base length of 120 mm whilst the fibre sensors measured strains on a much shorter base length, i.e. about 5 mm. These differences caused discrepancies between measurements. As predicted in Section 4, cracking was highly probable over a length of 11 cm – as confirmed in the tests – with a consequent strain increase; whereas over the 5 mm length concrete cracking was unlikely and so, much smaller strain values are detected. Data from unbonded fibre sensors were exploited because they could actually predict the plastic deformation of the steel rebars. In greater detail, Figure 13 shows that the maximum curvature at an amplitude of $2\delta_y$ was about 0.016 m^{-1}. By comparing this curvature value, that can also be seen as a capacity value, with the moment-curvature diagram of Figure 2b, it can be noted that FBGs provide information over the

nonlinear strain range, after cracks open. Figure 13b also shows that the estimate of the moment-curvature at $2\delta_y$ by means of the conventional strain gauge was not possible after attaining maximum deformation because it broke.

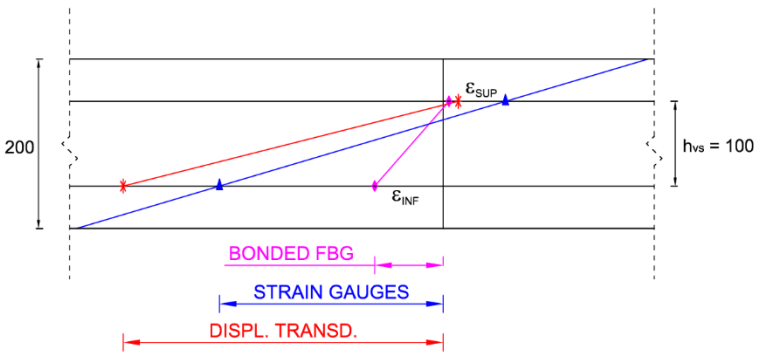

2δy CYCLE	ε_{SUP}	ε_{INF}
DISPL. TRANSD.	0.0003554	0.0075554
STRAIN GAUGES	0.001466	0.005279
BONDED FBG	0.000135	0.001616

Figure 12 SSC2 test: strains at the longitudinal rebar level for the 2δy cycle with bonded fibres. Dimensions in mm

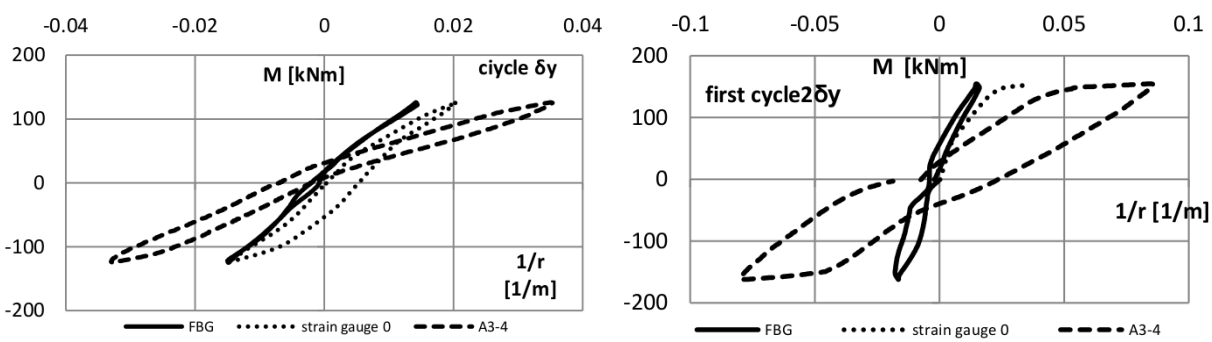

(a) (b)

Figure 13 SSC2 test: a) comparison of moment-curvature curve at amplitude δ_y, and b) comparison of moment-curvature curve at amplitude $2\delta_y$ with unbonded fibres

Figure 14 shows both the moment-rotation and the moment-curvature curve derived from the SSC3 test. The test was run up to the completion of cycles at $4\delta_y$. At those levels of displacement, the stiffness of the specimen was very low and most of the instrumentation could not correctly acquire owing to the presence of big cracks. A hysteretic behaviour owing to large energy dissipation is evident. In particular, Figure 15 highlights the performance of external fibres that measured strain values beyond 1% vs. standard concrete strain gauges that measured strain values up to 0.6%.

The performance of the external fibre packaging compared to both the internal fibre packaging and the conventional concrete strain gauges -see Figure 7c for the instrument

location- is depicted in Figure 16. The internal fibre packaging was made of a ribbed bar of the same material as the steel reinforcement as indicated in Figure 7c. Experimental data were obtained from the SSC4 test where both packages of fibre sensors were of the unbonded type. Both FBGs solutions could measure beyond 1% strain, and so, they were suitable for the target strain; conversely, common strain gauges accurately measured deformations corresponding to a cycle at ¾ δ_y of amplitude. The asymmetry of measurements shown in Figure 16b highlights again the problem of local cracks and consequent tension stiffening. In fact, Inf2 in tension measured different strain values compared to Inf1 and Inf0. In particular, only the strain gauge that was not involved in cracking worked up to cycles of $4\delta_y$ whilst the other two failed before deformation values of 5000 μm/m. From the analysis of negative strain measurements depicted in Figure 16, one can observe that the pre-strain applied to internal FBG sensors was not sufficient; in fact, it is more difficult to control a fibre directly installed on a steel bar. Conversely, an external installation permits a more accurate pre-strain control.

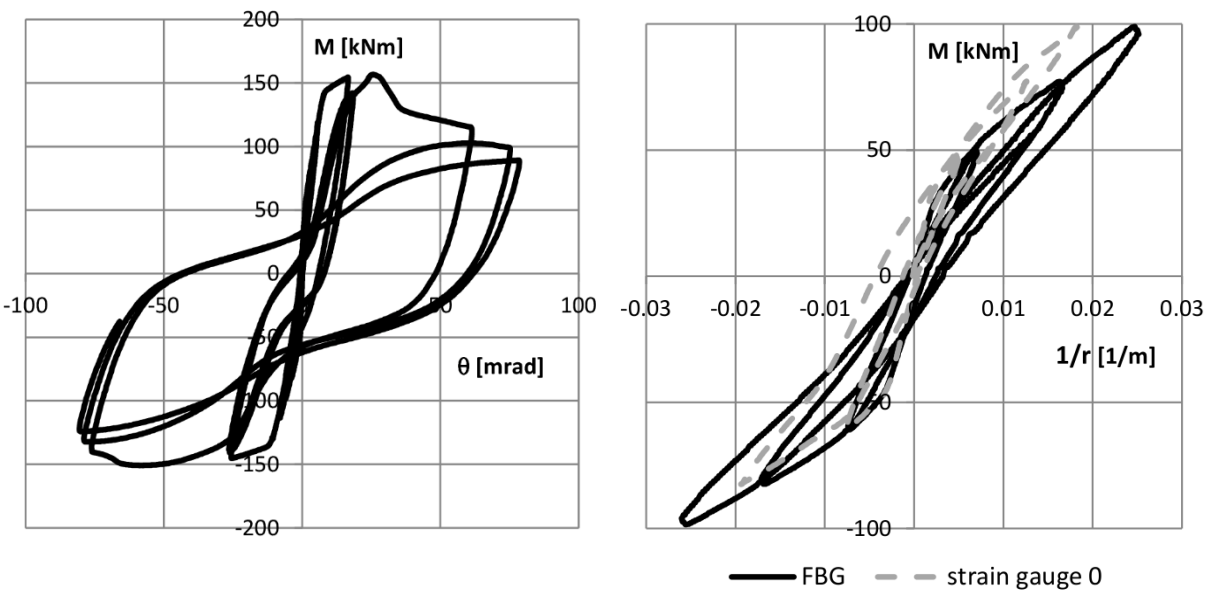

(a) (b)

Figure 14 SSC3 test endowed with external unbonded fibres: a) moment-rotation curve up to $4\delta_y$, and b) comparison of moment-curvature curve at amplitude δ_y

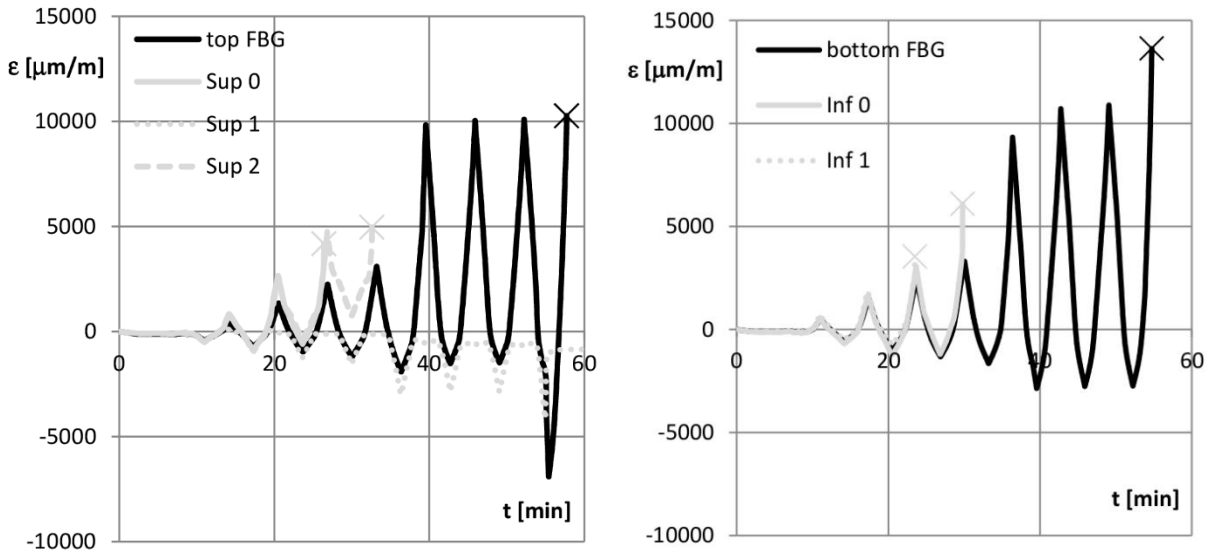

(a) (b)

Figure 15 SSC3 test: a) top, and b) bottom side unbonded external fibre data vs. conventional concrete strain gauges -Sup 0-2 and Inf 0-1.

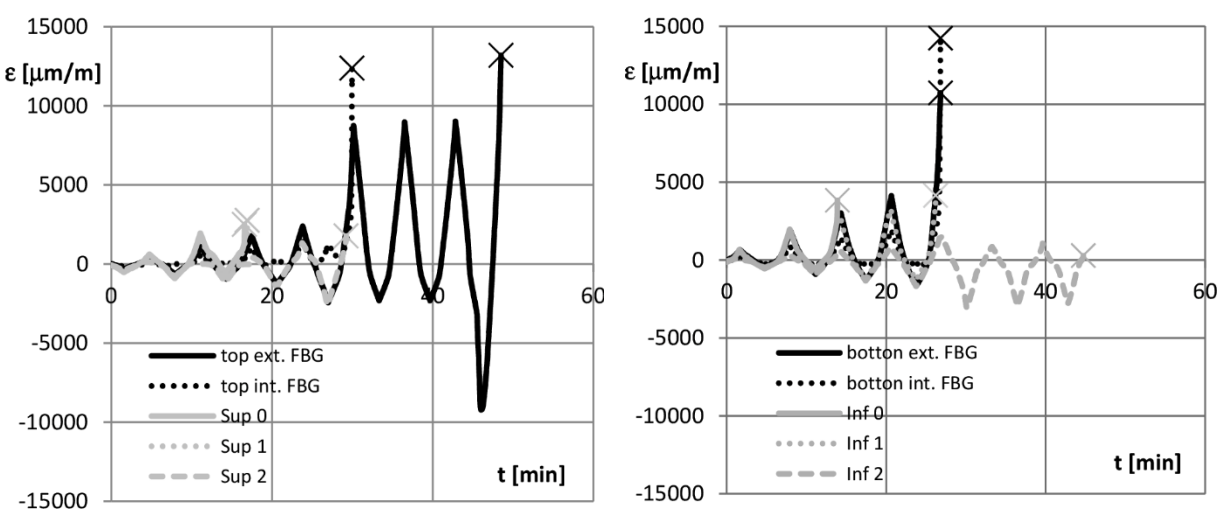

(a) (b)

Figure 16 SSC4 test: a) top, and b) bottom side FBG measurements vs. conventional strain gauges -Sup 0-2 and Inf 0-2.

In summary, from the tests carried out on substructures the following main conclusions can be drawn:

- The substructures exhibited a ductile behaviour characterized by large deformations in the plastic range associated with high energy dissipation, and hence the cross section used were suitable for seismic applications.
- In order to identify the seismic behaviour of a concrete section, average deformation measurements crossing cracks provide better information than

localized measurements. Short length strain measurements prevented an effective measurement of the cross-section behaviour because the strain field was underestimated owing to zones without cracks. In this respect, external and unbonded fibres provided average values that are more accurate.

- FBG sensors were capable of measuring larger deformations than conventional strain gauges. In particular, they measured higher strains than the target value of 1%; conversely, conventional concrete strain gauges always broke at strain values lower than 0.5%.
- In order to measure deformation in compression, FBG sensors needed a pre-strain that was better controlled with an external packaging.

On the basis of these results, both the internal and external unbonded solutions of FBGs were extensively employed in the full-scale specimen used in the TLC1 test mentioned in Section 3 and 4. Nonetheless, to get a complete picture of all packaging capabilities, Section #2 was also instrumented with embedded bonded fibres. When acquiring data from fibres the target resolution was selected as high as 1 microstrain and a maximum sampling rate of about 50 samples/sec was reckoned ideal for reproducing even the most rapid expected oscillation of a civil structure during an earthquake. The specimen was also instrumented with 16+4 standard displacement transducers and 6 load cells. Some strain values of this test are shown in Figure 17; FBG detected strain values up to 1.2% and confirmed the favourable performance of FBG sensors shown in substructure tests. Additional results can be found in [21].

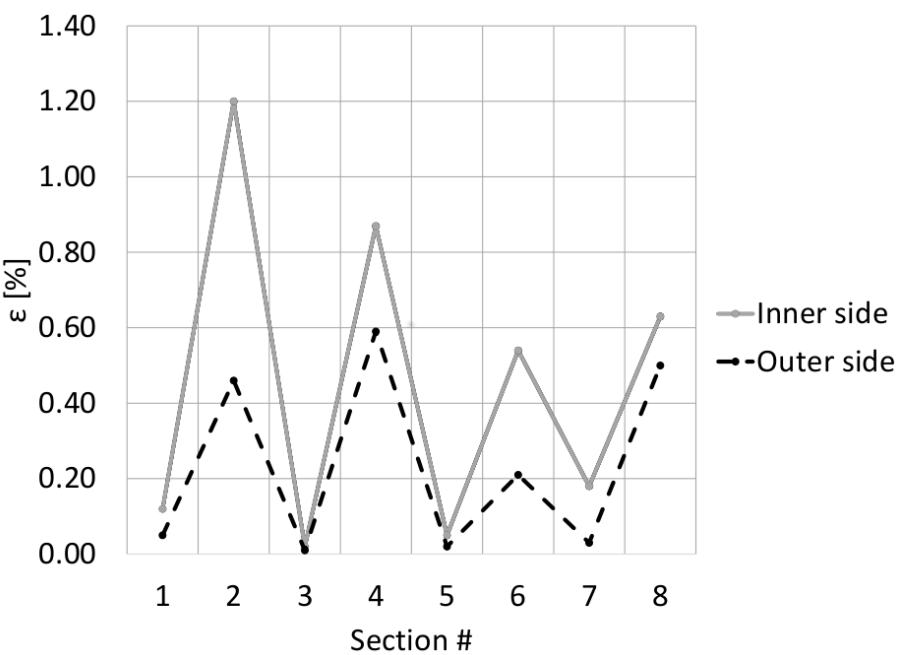

Figure 17 Maximum deformations of the tunnel lining at each instrumented section measured with FBG sensors

6 CONCLUSIONS

This paper investigated the capabilities of the optical fibre sensing technology based on Fibre Bragg Grating (FBG) to monitor the inelastic response of a circular tunnel lining located in a moderate seismic area. By means of an experimental campaign conducted on both substructure specimens and a full-scale test, several fibre packaging solutions were tested comprising bonded and unbonded sensors in concrete, internal (embedded) and external sensors.

The sensing unbonded solution both embedded and external performed reliably in the inelastic range for strains higher than 1%; this value was reckoned to be adequate for the deformation demands of ductile concrete sections typically located in moderate seismic-prone areas. These strains were measured both in the substructure tests and in the full-scale test. Thus, an unbonded fibre package is suited to structural health monitoring of civil infrastructures exhibiting a non-linear response. In fact, in the full-scale test, the FBG sensors were able to measure higher strain values at lining sections where plastic hinges formed; in particular, the internal unbonded FBG sensors approached a maximum strain value of about 1.2%. Nonetheless, an unbonded external solution for FBG packaging resulted to be preferable both for the simple sensor application/replacement during the construction process/service life and for a better control of fibre pre-straining.

ACKNOWLEDGMENTS

This work was carried out with a financial grant from the European Union Framework Programme 7 “Fibre optics-based intelligent monitoring and assessment system for proactive maintenance and seismic disaster prevention in reinforced concrete tunnel linings” (MONICO) FP7-SME-2007-1.

The support of AOS for the FBG acquisition during testing is gratefully acknowledged.

REFERENCES

1. Xiang JM, Liang M, Wavelet-based Detection of Beam Cracks Using Modal Shape and Frequency Measurements. *Computer-Aided Civil and Infrastructure Engineering* 2012; **27**(6): 439-454.
2. Hashash YMA, Hook JJ, Schmidt B, Yao JI-C, Seismic design and analysis of underground structures. *Tunnelling and Underground Space Technology* 2001; **16**: 247-293.
3. Wang JN, Seismic Design of Tunnels A Simple State-of-the-Art Design Approach. William Barclay Parsons Fellowshi, Parsons Brinckerhoff Monograph 7, 1993.
4. Penzien J, Wu CL, Stresses in linings of bored tunnels. *Earthquake Engineering and Structural Dynamics* 1998; **27**: 283-300.
5. Penzien J, Seismically induced racking of tunnel linings. *Earthquake Engineering and Structural Dynamics* 2000; **29**: 683-691.

6. Hashash YMA, Park D, Chiang Yao JI, Ovaling deformations of circular tunnels under seismic loading, an update on seismic design and analysis of underground structures. *Tunnelling and Underground Space Technology* 2005; **20**(5): 435-441.
7. Newmark NM, Problems in Wave Propagation in Soil and Rock, International Symposium on Wave Propagation and Dynamic Properties of Earth Materials, 1968.
8. Zhang W, Junqi G, Bin S, Heliang C, Health Monitoring of Rehabilitated Concrete Bridges Using Distributed Optical Fiber Sensing. *Computer-Aided Civil and Infrastructure Engineering* 2006; **21**(6):411–424
9. Moyo P, Brownjohn JMW, Suresh R, Tjin SC, Development of fiber Bragg grating sensors for monitoring civil infrastructure. *Engineering Structures* 2005; **27**(12):*1828–1834*.
10. Schroeck M, Ecke W, Graupner A, Strain Monitoring in steel rock bolts using FBG sensor arrays. *Proc SPIE* 2000; 4074: 298–304
11. Zhang Y, Li S, Yin Z, Chen B, Cui H-L, Ning J, Fiber-Bragg-grating-based seismic geophone for oil/gas prospecting. *Optical Engineering* 2006; **45**(8). DOI:10.1117/1.2337631
12. Tsuda H, Toyama N, Urabe K, Takatsubo J, Impact damage detection in CFRP using fiber Bragg gratings. *Smart Materials and Structures* 2004; **13**(4):719-724. DOI:10.1088/0964-1726/13/4/009
13. Nakamura K, Matsumura T, Ueha S, A load cell using a fiber Bragg grating with inherent mechanical temperature compensation. *Structural Control and Health Monitoring* 2005; **12**:345–355.
14. Lan C, Zhou Z, Ou J, Monitoring of structural prestress loss in RC beams by inner distributed Brillouin and fiber Bragg grating sensors on a single optical fiber. *Structural Control and Health Monitoring*, 2014. vol. 21, no. 3, pp. 317–330.
15. Rodrigues C, Félix C, Lage A, Figueiras J, Development of a long-term monitoring based on FBG sensors applied to concrete bridges. *Engineering Structures* 2011; **3**: 1993-2002.
16. Habel WR, Krebber K, Fiber-Optic sensor applications in civil and geotechnical engineering. *Photonic Sensors* 2011; **1**(3): 268-280.
17. Wu Z, Adewuyi AD, Identification of damage in reinforced concrete columns under progressive seismic excitation stages. *Journal of Earthquake and Tsunami* 2011; **5**(2): 151-165.
18. Majumder M, Gangopadhyay TK, Chakraborty AK, Dasgupta K, Bhattacharya DK, Fibre Bragg gratings in Structural Health Monitoring - Present status and applications. *Sensors and Actuators* 2008; **147**: 150-164.
19. Kerrouche A, Boyle WJO, Sun T, Grattan KTV, Schmidt JW, Taljsten B, Strain Measurement Using Embedded Fibre Bragg Grating Sensors Inside an Anchored Carbon Fiber Polymer Reinforcement Pre-stressing Rod for Structural Monitoring. *IEEE Sensors Journal* 2009; **9**(11): 1456-1461.
20. Loupos K, Kanellos G, Bursi OS, Frondistou S, Meissner J, Bairaktaris D, Griffoni B, Orfanoudakis A, Application of Fibre-Optic technologies for Real-

time Structural Monitoring - The MONICO EC Project, Proceeding of the 9th International Conference on Damage Assessment of Structures (DAMAS 2011), Oxford, UK, 11-13 July 2011.
21. Tondini N, Bursi OS, Bonelli A, Fassin M, Capabilities of a Fiber Bragg Grating Sensor System to Monitoring the Inelastic Response of Concrete Sections in New Tunnel Linings Subjected to Earthquake Loading. *Computer-Aided Civil and Infrastructure Engineering* 2014; Guest Editors: O.S. Bursi, M.Q. Feng and Z. Wu, 2014, Vol. 30, No. 8, 2015.
22. Kirzhner F, Rosenhouse G, Numerical analysis of tunnel dynamic response to earth motions. *Tunneling and Underground Space Technology* 2000; **15**(3): 249-258.
23. Ministero delle Infrastrutture, Norme Tecniche per le Costruzioni, 2008 (in Italian).
24. Chai YH, Romstad KM, Bird S, Energy Based Linear Damage Model for High-Intensity Seismic Loading. *Journal of Structural Engineering, ASCE* 1995; **121**(5): 857-864.
25. Bursi OS, Ferrario F, Computational Models for the Low-cycle Fatigue Behaviour of Composite Members and Joints, in *Progress in Civil and Structural Engineering Computing*, Edited by B.H.V. Topping, Saxe-Coburg Publications, Stirling 2003; pp. 119-148.
26. Park YJ, Ang AH-S, Mechanistic seismic damage model for reinforced concrete, *Journal of Structural Engineering*, ASCE 1985; **111**(ST4): 722-739.
27. Park YJ, Ang AH-S, Wen YK, Damage-limiting aseismic design of buildings, *Journal of Structural Engineering*, ASCE, 1987; **3**(1): 1-26.
28. Nilson AH, Winter G, *Design of Concrete Structures* 10 th Ed. McGraw, Hill, New York etc. 1986
29. Ordinanza del Presidente del Consiglio dei Ministri N. 3274 e s.m. (3431 3 maggio 2005). Primi elementi in materia di criteri generali per la classificazione sismica del territorio nazionale e di normative tecniche per le costruzioni in zona sismica, 20 marzo 2003 (in Italian).
30. Technical Committee 1, TWG 1.3, Recommended testing procedures for assessing the behaviour of structural steel elements under cyclic loads ECCS, No. 45, 1986.
31. CEN Eurocode 2 Design of concrete structures. General rules and rules for buildings. EN 1992-1, European Committee for Standardization, Brussels, Belgium, 2005.

Table 1
Maximum and minimum characteristic values of internal actions based on Penzien and Wu theory [4]

Stress	Max	Min
Bending moment [kNm/m]	84.38	-84.38
Thrust force [kN/m]	-640.25	-780.89
Shear action [kN/m]	69.25	-69.25

Table 2 Test programme and Fibres combinations used in different tests

Test		*Testing Procedure*	*Specimen/Test acronym*	*Notes about fibres*
Substructure Tests	1	Monotonic	SSM1	No fibre
	2	Cyclic ECCS	SSC1	No fibre
	3	Cyclic ECCS	SSC2	Internal bonded and unbonded FBG fibres
	4	Cyclic ECCS	SSC3	External unbonded FBG fibres
	5	Cyclic ECCS	SSC4	Internal and external unbonded FBG fibres
	6	Cyclic ECCS	SSC5	External unbonded Brillouin fibres
Test on Tunnel Lining		Cyclic ECCS	TLC1	FBGs with various configurations